Performance improvement of the RSM970S radar speed controller of ASECNA, Douala International Airport

Moussa Bessike Angon, Offolé Florence, Nguiya Séverin, Moune Cédric Jordan, Ndoumbé Matéké Max

Energy, Materials, Modelling, and Methods Research Laboratory (LE3M), National Higher Polytechnic School of Douala,
University of Douala, Douala, Cameroon

Article Info	ABSTRACT
	This article addresses the direct torque control associated with artificial intelligence for the control of the RSM970S radar of The Agency for the Safety of Air Navigation in Africa and Madagascar (ASECNA), Douala International Airport. The radar is driven by two identical induction motors powered by a single inverter. Direct torque control is associated with fuzzy logic and artificial neural networks. The test results performed in MATLAB/Simulink showed an improvement in the dynamic performance of the drive system compared to a conventional direct torque control. There is an overshoot in speed during the steady state of less than 0.955% of the neural technique over the fuzzy technique. But also, an accuracy of 99.58% of the two techniques proposed in this article. These results ensure good precision and stability of the radar in the detection of airplanes in the Cameroonian airspace.

Corresponding Author:

Ndoumbé Matéké Max
Energy, Materials, Modelling, and Methods Research Laboratory (LE3M)
National Higher Polytechnic School of Douala, University of Douala
Carrefour Ange Raphaël, Douala 2701, Cameroon
Email: mdesmax@yahoo.fr

1. INTRODUCTION

The improvement of air navigation safety is a major problem in airports around the world in general, and at Douala International Airport in particular [1]-[11]. It was also the subject of an international conference of the International Union of Radio Telecommunications in conjunction with the International Civil Aviation Organization (ICAO) whose aim was to strengthen flight safety in the airspace under the control of Agency for the Safety of Air Navigation in Africa and Madagascar (ASECNA). In 2017, ASECNA, Cameroon acquired the RSM970S radar at Douala International Airport, following the Mbanga Pongo disaster of May 5, 2007, which killed several people. Subsequently, the application of the recommendations of ICAO led ASECNA to equip its radar with a speed control device for the precision of the detection of aircraft circulating in the airspace placed under the control of Douala International Airport [7], [8], [11]. This service replaces traditional methods, by control modules integrating direct torque control (DTC) [12]-[15] to achieve coordination and synchronization between the two induction motors that drive the rotation of the taxes of movement ensuring the rotation of the radar aerial RSM970S of the manufacturer Thales. The ASECNA radar system consists of a permanently rotating antenna installed at the end of the landing runway, a data processing system received from the antenna, and a display screen [16]. The rotation seed of the antenna is chosen so as to follow the trajectory of the planes once they enter the airspace under the control of ASECNA Douala. This rotation speed is fixed jointly between the Cameroon Civil Aviation Authority (CCAA) and ASECNA according to the air traffic.

Furthermore, the permanent rotation antenna subsystem, located in a free and open space, is subject to very strong winds that add a rotational influence to the antenna, thus modifying the initial set point which is 12 revolutions in 5 minutes. To maintain this constant rotation speed, a DTC-controlled speed regulation device was added. The sudden change in direction and speed of the wind at Douala International Airport is a major problem for the rotation of the radar supposed to have a constant rotation speed, a problem for which ASECNA is struggling to find a definitive solution. The approaches used so far to stabilize the radar rotation have been, firstly, the use of a stepper motor, the disadvantage being that it has a particularly penalizing electrical power at high speed, due to the rapid back and forth of energy to which the power supply is subjected. Another approach was the use of direct current motors [17], this type of motor has the disadvantage that the wear of the brushes, the degradation of the surface condition of the collectors, the pollution by the coal dust are parameters that influence negatively on the proper functioning. These solutions have been abandoned in favor of a speed variator consisting of two induction motor drives whose control law is based on conventional DTC which, to date, has not produced the expected effect supposed to maintain a constant speed of 12 revolutions in five minutes [18], [19].

This study provides a solution to the problem as described. It consists of improving the dynamic performances of conventional DTC by using artificial intelligence techniques. The association of conventional DTC with artificial intelligence brings a better improvement of the torque and magnetic flux ripples, which guarantees a better precision to the radar keeping it constant with respect to the set point. A clear stabilization of the switching frequency constant is also observed, which facilitates the control of the energy concentrated on a given frequency range.

2. SYSTEM DESCRIPTION AND MODELLING

The radar drive is ensured by a mechanism composed of two identical three-phase induction motors each associated with a reducer as shown in Figure 1. These motors are powered via a single three-phase inverter. This segmentation of the transit of mechanical power allows the system to operate in degraded mode in case of a fault in one of the two motors, this increases the overall reliability of the system, an important parameter for a sensitive application such as air surveillance.

2.1. Model of the three-phase asynchronous motor

The state model of the induction machine is given by the relation, as in (1) [20].

$$\dot{X} = AX + BU \tag{1}$$

With (2), and $\sigma = (1 - \frac{M^2}{L_s L_r})$ is the Blondel coefficient.

$$
\underbrace{\begin{bmatrix} \dot{I}_{s\alpha} \\ \dot{I}_{s\beta} \\ \dot{\varphi}_{s\alpha} \\ \dot{\varphi}_{s\beta} \end{bmatrix}}_{\dot{X}} = \underbrace{\begin{bmatrix} -\left(\frac{R_s}{\sigma L_s} + \frac{R_r}{\sigma L_r}\right) & -\omega & \frac{R_r}{\sigma L_s L_r} & \frac{\omega}{\sigma L_s} \\ \omega & -\left(\frac{R_s}{\sigma L_s} + \frac{R_r}{\sigma L_r}\right) & -\frac{\omega}{\sigma L_s} & \frac{R_r}{\sigma L_s L_r} \\ -R_s & 0 & 0 & 0 \\ 0 & -R_s & 0 & 0 \end{bmatrix}}_{A} \underbrace{\begin{bmatrix} I_{s\alpha} \\ I_{s\beta} \\ \varphi_{s\alpha} \\ \varphi_{s\beta} \end{bmatrix}}_{X} + \underbrace{\begin{bmatrix} \frac{1}{\sigma L_s} & 0 \\ 0 & \frac{1}{\sigma L_s} \\ 0 & 0 \\ 0 & 0 \end{bmatrix}}_{B} \underbrace{\begin{bmatrix} V_{s\alpha} \\ V_{s\beta} \end{bmatrix}}_{U} \tag{2}
$$

The expression of the electromagnetic torque is given by (3) [20].

$$C_{em} = \frac{3}{2} p \left(\varphi_{s\alpha} I_{s\beta} - \varphi_{s\beta} I_{s\alpha} \right) \tag{3}$$

The mechanic equation of the machine by (4) [20].

$$C_{em} - C_r = J \frac{d\Omega(t)}{dt} + f\Omega(t) \tag{4}$$

With R_s and L_s; R_r; and M; ω; p; J and f respectively: Static resistance and static inductance, rotatory inductance; mutual inductance; the rotor frequency; the number of pairs of poles of the machine; the moment of inertia, and the viscous friction coefficient. But also, aussi $V_{s\alpha,\beta}$; $I_{s\alpha,\beta}$ and $\varphi_{s\alpha,\beta}$ respectively stator voltages, currents, and fluxes in the complex plane (α, β) and $\Omega(t)$ the rotation speed of the machine.

2.2. Voltage inverter model

The power supply of the actuators is ensured through a two-level voltage inverter (3 arms/6 switches), whose matrix representation so give as (5) [21], [22].

$$\begin{bmatrix} V_{sa} \\ V_{sb} \\ V_{sc} \end{bmatrix} = \frac{V_{dc}}{3} \begin{bmatrix} 2 & -1 & -1 \\ -1 & 2 & -1 \\ -1 & -1 & 2 \end{bmatrix} \begin{bmatrix} S_a \\ S_b \\ S_c \end{bmatrix} \tag{5}$$

With V_{dc} the value of the DC bus voltage and S_a, S_b, and S_c control signals of the inverter arms of the modulator. This matrix representation is used to derive the control vector for the machine's three phases, in order to satisfy its energy demand. The control system is vector-based, making it easy to implement and share energy across machines powered by the same inverter.
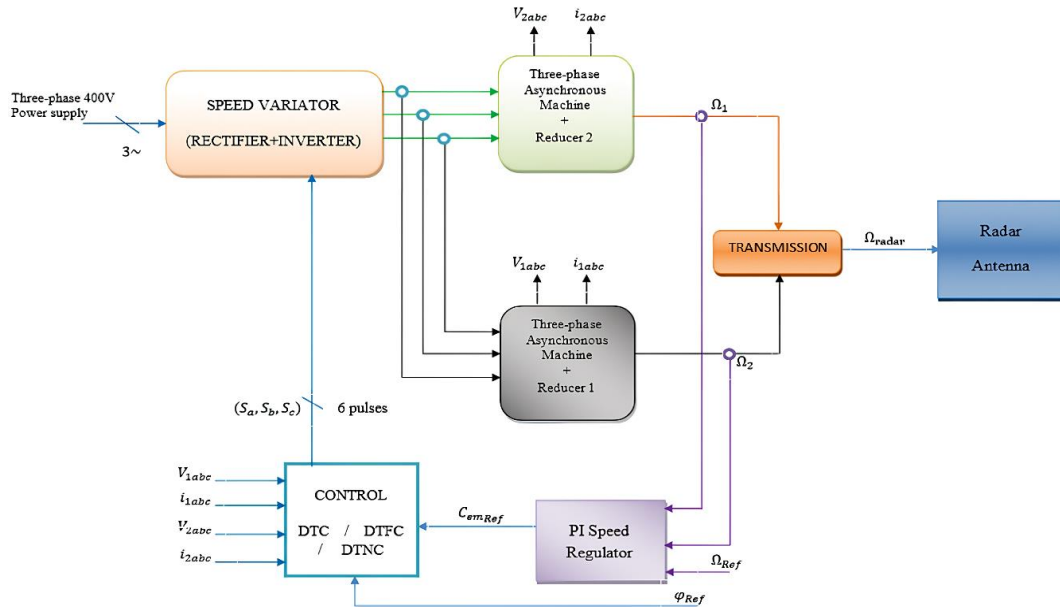
Figure 1. Radar drive system RSM970S trainer

3. ARTIFICIAL INTELLIGENCE BASED DTC DEVELOPMENT
3.1. Fuzzy logic direct torque control

The principle of direct torque fuzzy control (DTFC) is based on a fuzzy controller instead of the hysteresis controllers and the Takahashi table. The controller has 03 inputs: $\Delta\varphi_s$, ΔC_{em}, and θ_s; and as outputs the control signals S_a, S_b, and S_c [23], [24]. The controller used is of the Mamdani type and its design involves fuzzification of the variables. $\Delta\varphi_s$ is divided into two fuzzy sets (N and P); ΔC_{em} three fuzzy sets (N, Z, and P) and θ_s in six fuzzy sets such that: $-\frac{\pi}{6} + i\frac{\pi}{3} \leq \theta_i \leq \frac{\pi}{6} + i\frac{\pi}{3}$ with $i \in [1; 6]$. Figure 2 shows the fuzzification strategy of the inputs of our proposed controller. Figure 2(a) shows the flux error membership function, Figure 2(b) shows the torque error membership function, from which the torque control law is defined. Finally, Figure 2(c) shows the position of the stator flux vector. We note: N = negative; Z= zéro et P = positive.
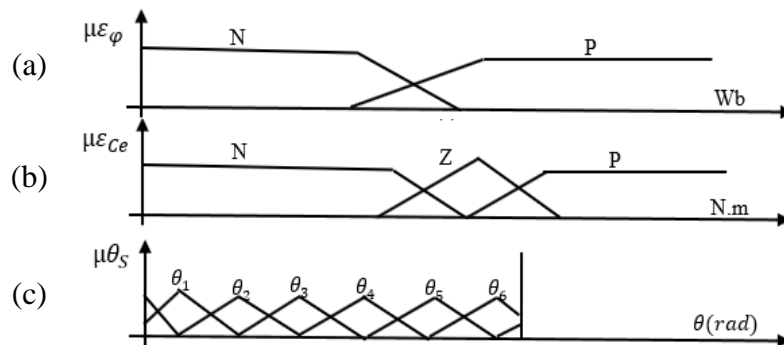

Figure 2. The strategy of fuzzification of the entries: (a) flow error membership function, (b) torque error membership function, and (c) position of stator flux vector

The behavior of the controller is guided by a set f rules such that each rule makes a map between the state of entry values and exit values depending on the model: R_i: If ε_φ is A_i and $\varepsilon_{C_{em}}$ is B_i and θ_s is C_i then S_k is V_i. With A_i B_i and C_i which represent the linguistic variables of the stator flux error, the torque error, and the position of the stator flux vector. V_i represents the linguistic variable of the output and R_i the rule number i (ranging from 1 to 36) [23], [25], [26].

3.2. Neural direct torque control strategy

To achieve the direct torque neural control (DTNC), the neural controller replaces the selection table of the conventional DTC control and therefore has as inputs: Kcem; Kφ; and θs and as outputs: S_a, S_b; and S_c. The training of the neural network is done by supervised learning, and the chosen learning algorithm is that of backpropagation of the error. During the training of the network with the data provided by the simulation of the conventional DTC control, when data is presented at the input of the network, the output is obtained by a calculation propagated from the input layer to the output layer [24]. The quadratic sum of errors is thus obtained by (6) [14].

$$E(k) = \frac{1}{N} \sum_{i=1}^{N} \big(d_i(k) - y_i(k)\big)^2 \qquad (6)$$

With: d_i The desired output; y_i The calculated output; k The number of iterations and N The number of data from the training base.

Thus, following the method of backpropagation of the error, the error is propagated from the output to the inputs causing a modification of the synaptic coefficients of the network, and refining the precision of the controller at each iteration. The neural controller in this study is a network of 3 layers structured in 3-15-3, whose first layer is activated by a sigmoid function (logsig), the second one activated by a sigmoid function (tansig), and the last one by a linear function (purelin). Figure 3 shows the structure of the controller under the MATLAB/Simulink environment.

The chosen optimization method is that of Levenberg-Marquardt for its speed and convergence. The network training was carried out with 15,000 iterations and for an error of 10^3. Once the learning is completed, the neural controller provides outputs equal or approximate to those expected according to the value of the input data.
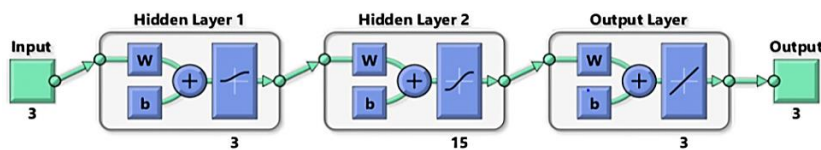

Figure 3. Neuronal controller

4. SIMULATION AND RESULT ANALYSIS

Three controls have been tested, all three based on the principle of direct torque control: the conventional DTC control, the fuzzy DTC control, and the neural DTC control. A resistive torque of 10N.m applied throughout the simulation represents the resistance force that the wind imposes on the rotation of the radar antenna. In accordance with the technical document provided by ASECNA, we have chosen a 7.5 kW motorization among the models available from MATLAB/Simulink. The 7.5 kW motor chosen has the parameters described in Table 1.

Table 1. Simulation parameters of the machine

Parameters	Values	Parameters	Values
Stator résistance	0.7384 Ω	Nominal power	7.5 kW/ 400 V; 50 Hz
Rotor résistance	0.7402 Ω	Number of pole pairs	2
Stator inductance	0.003045 H	Inertia moment	0.0343 kg.m²
Rotor inductance	0.003045H	Viscous friction coefficient	0.000503
Mutual inductance	0.1241 H	Reducer	10
Nominal speed	1440 tr/min		

The speed set point is set so that the radar plate makes 12 revolutions in five minutes or 2.4 rpm. This value corresponds to a very low-speed operation of the motors (2.4 rpm × 2 × pi ×10 /60 = 2.51 rad/s), despite the reducer with a ratio of 10. Thus, the fastest response is obtained with the conventional DTC control as shown in Figure 4(a), and followed by the DTNC control as shown in Figure 4(b). The DTFC control is the slowest with a longer transient phase as shown in Figure 4(c).
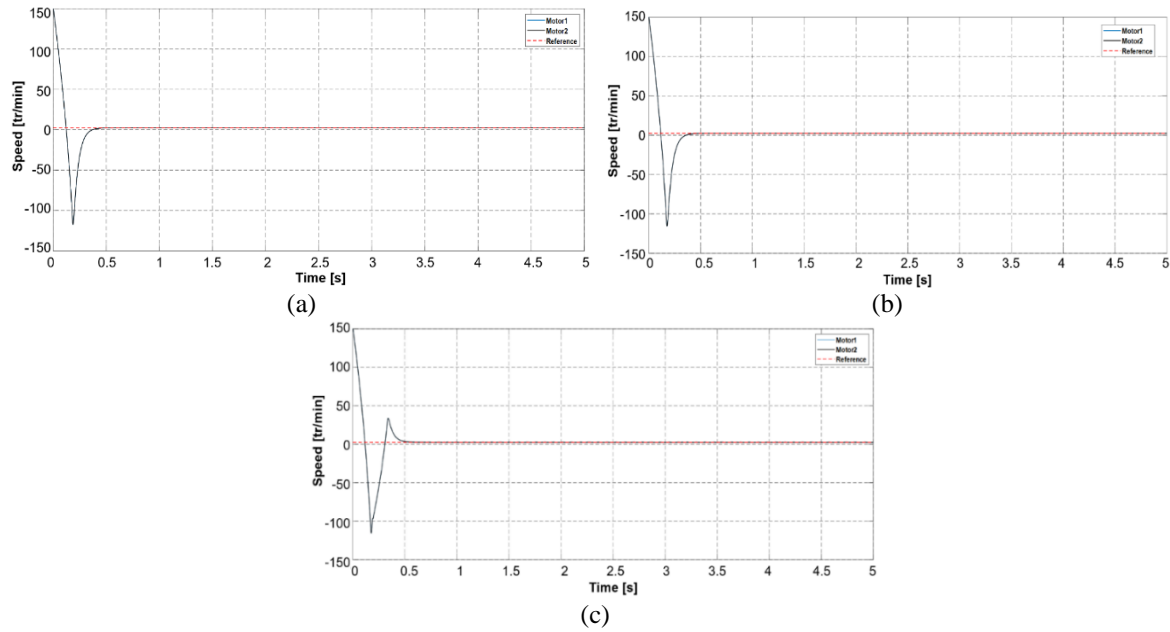
(a)

(b)

(c)

Figure 4. Rotation speed: (a) C-DTC, (b) DTNC, and (c) DTFC

The oscillations of the electromagnetic torque have an effect on the dynamics of the rotation speeds of the motors and consequently on that of the radar. With the conventional DTC control, the motor speed has the most noise as shown in Figure 5(a), compared to the fuzzy DTC control as shown in Figure 5(b), and the neural DTC control whose response is the least polluted as shown in Figure 5(c). These noises or parasites result in significant mechanical vibrations leading to wear of the motor shaft in the long term, but above all this influences the precision of the radar.

(a)

(b)

(c)
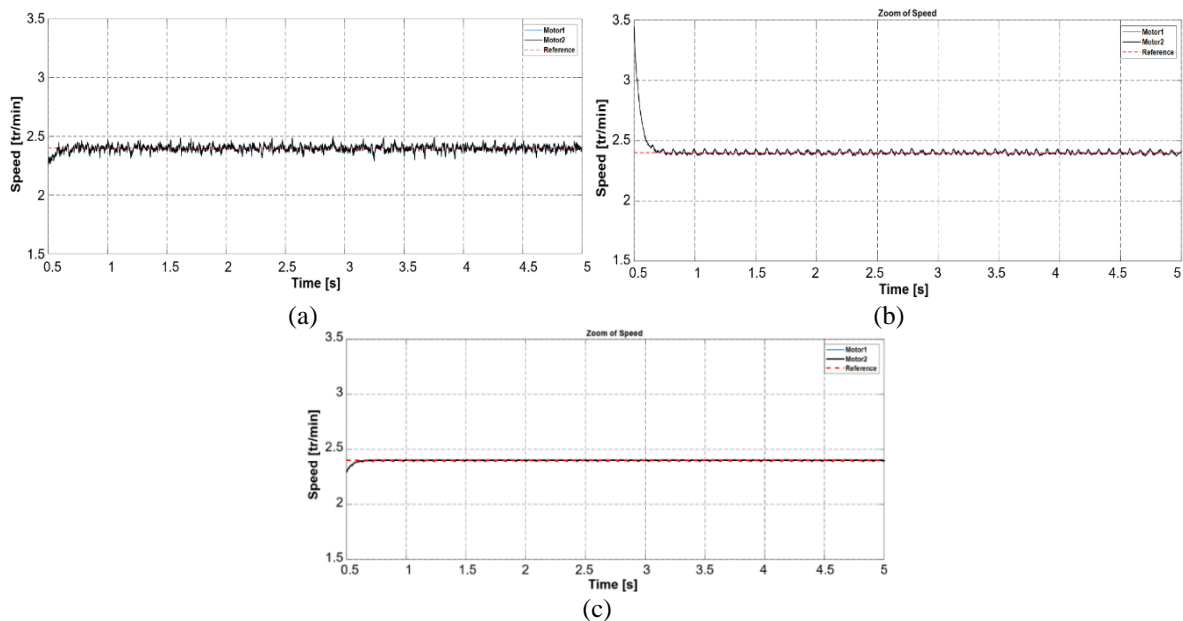
Figure 5. Zoom speed of rotation: (a) C-DTC, (b) DTFC, and (c) DTNC

The chosen hysteresis band is [-2N.m, 2N.m]. At start-up, torques reach a maximum value of 80 N.m, before returning to the set value of 10 N.m for all three controls. Nevertheless, the conventional DTC control exhibits high oscillations as shown in Figure 6(a). The DTFC and DTNC controls are the most robust, with oscillations perfectly maintained within the set tolerance range, as shown in Figures 6(b) and 6(c).
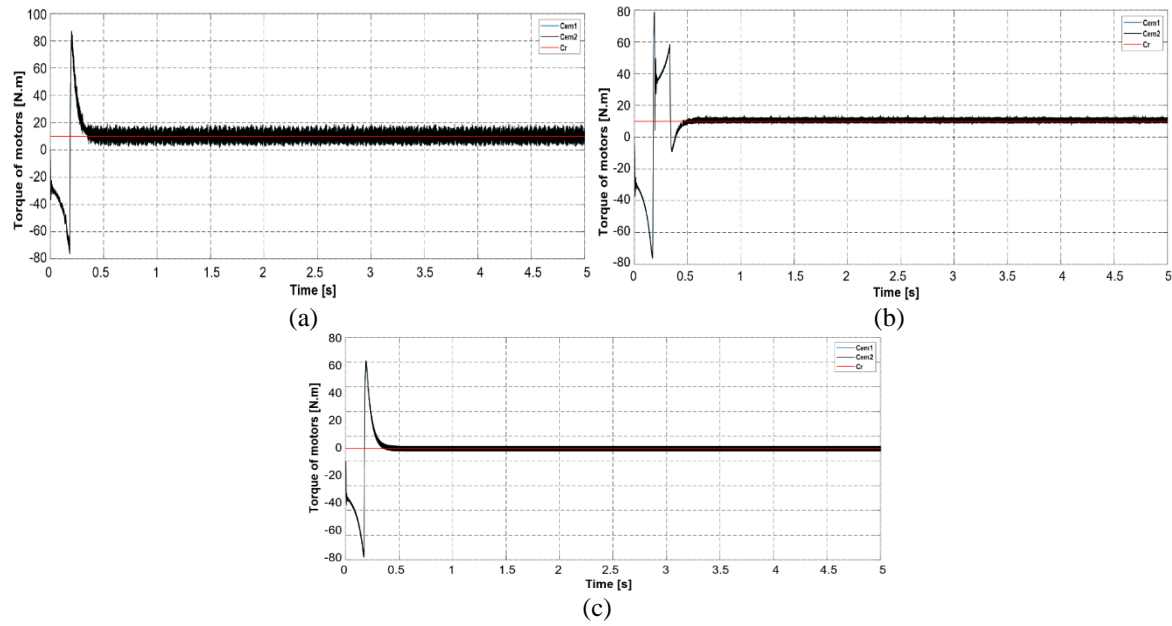
Figure 6. Electromagnetic couple: (a) C-DTC, (b) DTFC, and (c) DTNC

This enabled us to evaluate the number of revolutions made by the radar antenna after five minutes. Figure 7(a) shows that the radar antenna makes just 10.2 turns in five minutes, giving an accuracy of 85%. Looking at Figures 7(b) and 7(c), we can see that for each of the two commands, the radar antenna completes 11.95 revolutions in 5 minutes, giving an accuracy of 99.58 %.
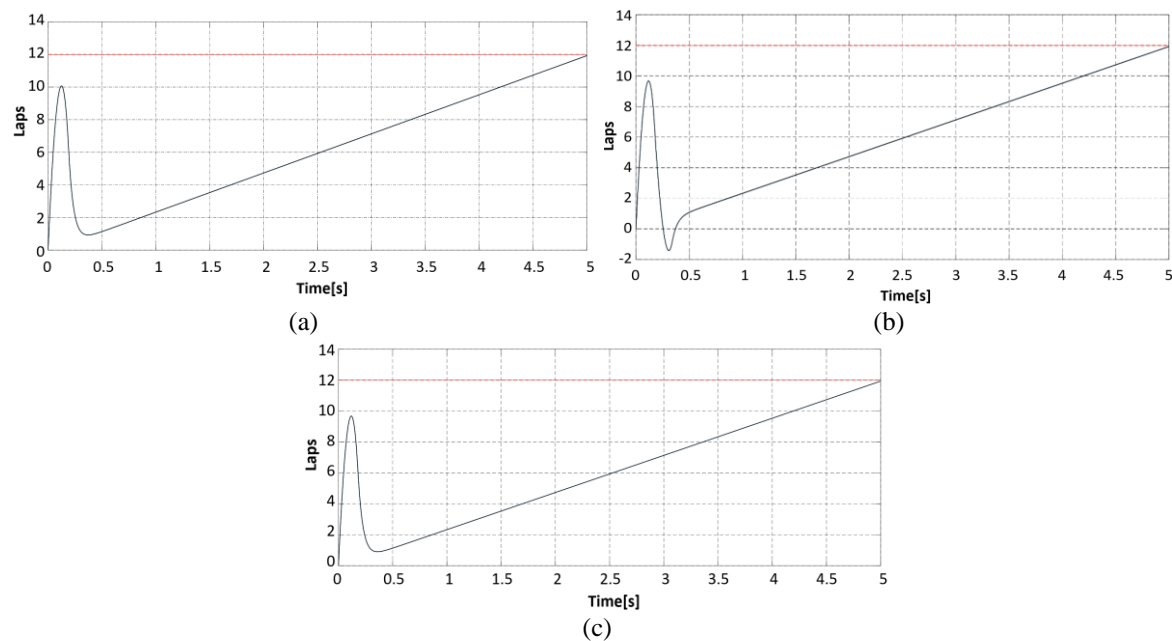

Figure 7. Number of turns: (a) C-DTC, (b) DTFC, and (c) DTNC

At start-up the amplitude of the stator currents reaches 100A, and in the steady state, they have a more or less sinusoidal form for the three drives used. Sinusoidal shape for the three drives used. With conventional DTC control, the shape of the stator of the stator currents is more distorted as shown in Figure 8(a), unlike the less polluted DTNC control as shown in Figure 8(b). The DTFC control has the best waveform with a longer transient phase as shown in Figure 8(c).
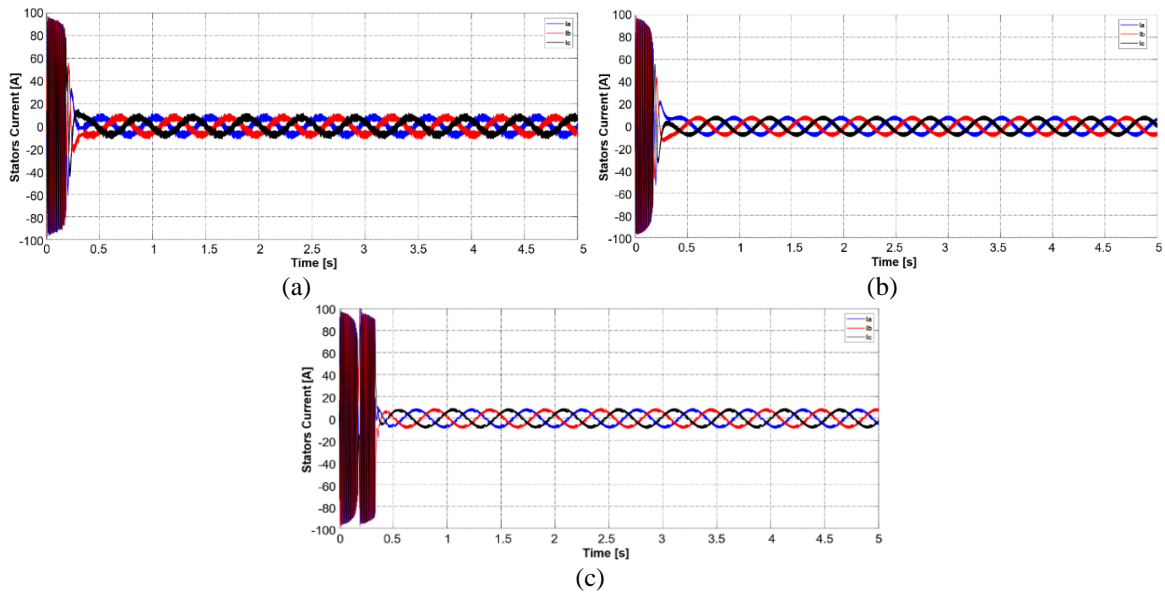
Figure 8. Stator currents: (a) C-DTC, (b) DTNC, and (c) DTFC

The stator flux modulus setpoint is fixed at 0.6Wb, with a tolerance range of [-0.01 Wb; 0.01Wb]. Stator flux oscillations are very high with conventional DTC control Figure 9(a). With DTNC and DTFC control, the oscillations are perfectly maintained within the band as shown in Figures 9(b) and 9(c). Table 2 gives the quantifiable values for each proposed control method. From this table it can be seen that the techniques based on approaches with artificial intelligence provide greater stability and accuracy for the radar. This guarantees good detection of aircraft in the airspace.
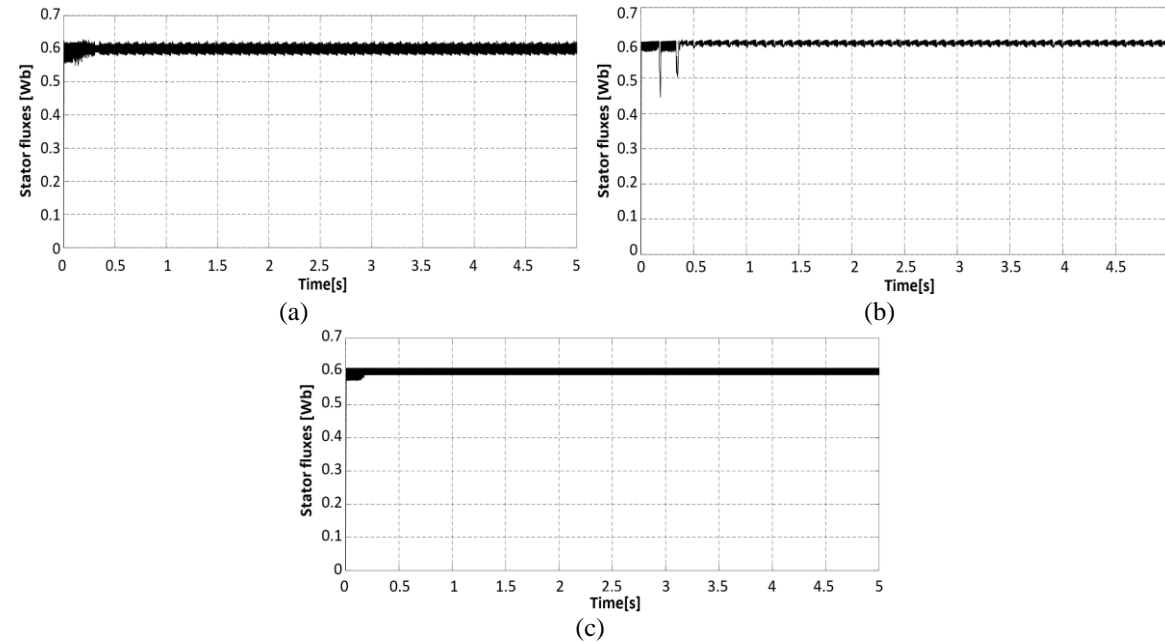
Figure 9. Stator flux modulus: (a) C-DTC, (b) DTFC, and (c) DTNC

Table 2. Comparative table of the different methods proposed

Commands	DTC convention	DTFC	DTNC	Commands	DTC convention	DTFC	DTNC
Response time 5% (s)	0.575	0.7525	0.688	Torque overrun (%)	68	00	00
Speed overrun (%)	3.54	1.33	0.375	Flux oscillations (Wb)	0.0309	0.0145	0.02
Torque oscillations (N.m)	6.72	4.00	4.00	Flux overrun (%)	104.5	00	00

5. CONCLUSION

Here, the use of artificial neural networks and fuzzy logic is employed to improve the drive system of ASECNA's RSM 970S airport radar in Douala, which comprises two identical induction motors driven by a conventional DTC. The results show an improvement in radar accuracy and stability, a reduction in the amplitudes of torque ripples and motor flux, and a consequent reduction in jerks (sudden shocks). The results obtained in this article show that torque and flux overshoots are zero for the DTFC and DTNC control strategies. The simulations carried out for an operating time of 5 minutes, correspond to the set point of the radar plate. The prospects for improvement in this work lie in the field of merging control techniques, such as the combination of neuro-flow (with or without compensation), and genetic algorithms.

REFERENCES

[1] F. A. Butt and M. Jalil, "An overview of electronic warfare in radar systems," in *2013 The International Conference on Technological Advances in Electrical, Electronics and Computer Engineering (TAEECE)*, 2013, pp. 213–217. doi: 10.1109/TAEECE.2013.6557273.

[2] A. D. Iohimovich, A. V. Korovin, and V. V. Pankratov, "The development of the direct electric drive system of a radar station antenna," in *2013 14th International Conference of Young Specialists on Micro/Nanotechnologies and Electron Devices*, IEEE, Jul. 2013, pp. 300–304. doi: 10.1109/EDM.2013.6642000.

[3] V. F. Strelkov and M. V. Andryukhin, "Peculiarities of operation of radar antenna variable speed electric drive," in *2018 International Conference on Industrial Engineering, Applications and Manufacturing (ICIEAM)*, 2018, pp. 1–5. doi: 10.1109/ICIEAM.2018.8728678.

[4] R. Blázquez-García, D. Cristallini, M. Ummenhofer, V. Seidel, J. Heckenbach, and D. O'Hagan, "Capabilities and challenges of passive radar systems based on broadband low-Earth orbit communication satellites," *IET Radar, Sonar & Navigation*, vol. 18, no. 1, pp. 78–92, Jan. 2024, doi: 10.1049/rsn2.12446.

[5] V. F. Strelkov, V. V. Vanyaev, I. V. Bobyliov, and M. V. Andryukhin, "Control method and system of a radar antenna rotation electric motor," *RU patent*, p. 18, 2015.

[6] J. Sun, Y. Yuan, Y. Wang, X. Yang, and W. Yi, "Enumeration PCRLB-based power allocation for multitarget tracking with colocated MIMO radar systems in clutter," *IEEE Transactions on Geoscience and Remote Sensing*, vol. 61, 2023, doi: 10.1109/TGRS.2023.3278727.

[7] G. Longo, E. Russo, A. Armando, and A. Merlo, "Attacking (and defending) the maritime radar system," *IEEE Transactions on Information Forensics and Security*, vol. 18, pp. 3575–3589, 2023, doi: 10.1109/TIFS.2023.3282132.

[8] J. Wang, T. Yi, X. Liang, and T. Ueda, "Application of 3D laser scanning technology using laser radar system to error analysis ian the curtain wall construction," *Remote Sensing*, vol. 15, no. 1, p. 64, Dec. 2022, doi: 10.3390/rs15010064.

[9] Y. Song, L. Hua, K. Yan, W. Han, P. Zhu, and Z. Ye, "Research on fault diagnosis method of radar antenna transmission gear based on motor current characteristics," *Journal of Physics: Conference Series*, vol. 2296, no. 1, Jun. 2022, doi: 10.1088/1742-6596/2296/1/012003.

[10] Y. Á. López, M. García-Fernández, G. Álvarez-Narciandi, and F. L.-H. Andrés, "Unmanned aerial vehicle-based ground-penetrating radar systems: A review," *IEEE Geoscience and Remote Sensing Magazine*, vol. 10, no. 2, pp. 66–86, Jun. 2022, doi: 10.1109/MGRS.2022.3160664.

[11] D. V. I. Bota and T. Petrița, "An upgrade of MIT SAR radar project," in *2023 17th International Conference on Engineering of Modern Electric Systems (EMES)*, IEEE, Jun. 2023, pp. 1–4. doi: 10.1109/EMES58375.2023.10171626.

[12] I. Takahashi and Y. Ohmori, "High-performance direct torque control of an induction motor," *IEEE Transactions on Industry Applications*, vol. 25, no. 2, pp. 257–264, 1989, doi: 10.1109/28.25540.

[13] N. M. Max *et al.*, "Artificial intelligence-enhanced DTC command methods used for a four-wheel-drive system," *International Journal of Power Electronics and Drive Systems (IJPEDS)*, vol. 14, no. 4, pp. 1983–1994, Dec. 2023, doi: 10.11591/ijpeds.v14.i4.pp1983-1994.

[14] N. M. Max, N. Y. J. Maurice, E. Samuel, M. C. Jordan, A. Biboum, and B. Laurent, "DTC with fuzzy logic for multi-machine systems: traction applications," *International Journal of Power Electronics and Drive Systems (IJPEDS)*, vol. 12, no. 4, pp. 2044–2058, Dec. 2021, doi: 10.11591/ijpeds.v12.i4.pp2044-2058.

[15] N. El Ouanjli *et al.*, "Modern improvement techniques of direct torque control for induction motor drives - a review," *Protection and Control of Modern Power Systems*, vol. 4, no. 2, pp. 1–12, Dec. 2019, doi: 10.1186/s41601-019-0125-5.

[16] S. S. Parit and V. G. Kasabegoudar, "Ultra wideband antenna with reduced radar cross section," *International Journal of Electromagnetics and Applications*, vol. 6, no. 2, pp. 23–30, 2016, doi: 10.5923/j.ijea.20160602.01.

[17] V. Rahmati and A. Ghorbani, "A novel low complexity fast response time fuzzy pid controller for antenna adjusting using two direct current motors," *Indian Journal of Science and Technology*, 2018, doi: 10.17485/ijst/2018/v11i13/171604.

[18] G. Banda and S. G. Kolli, "Comparison of ANN- and GA-based DTC eCAR," *Journal of Power Electronics*, vol. 21, no. 9, pp. 1333–1342, Sep. 2021, doi: 10.1007/s43236-021-00273-1.

[19] B. Chinthamani, S. Kavitha, N. S. Bhuvaneswari, and N. R. Shanker, "Induction motor torque prediction using dual function radar received polarised signals and machine learning algorithm," *Journal of Electrical Engineering & Technology*, vol. 18, no. 5, pp. 3733–3741, Sep. 2023, doi: 10.1007/s42835-023-01470-7.

[20] W. Zhou, M. Diab, X. Yuan, L. Xie, J. Wang, and Z. Zhang, "Inverter with paralleled modules to extend current capacity and combat motor overvoltage in SiC-based adjustable speed drives," *IEEE Transactions on Industrial Electronics*, vol. 71, no. 5, pp. 4474–4484, May 2024, doi: 10.1109/TIE.2023.3281709.

[21] M. Cacciato, A. Consoli, G. Scarcella, and A. Testa, "Reduction of common-mode currents in PWM inverter motor drives," *IEEE Transactions on Industry Applications*, vol. 35, no. 2, pp. 469–476, 1999, doi: 10.1109/28.753643.

[22] A. Cheriti, K. Al-Haddad, L. Dessaint, D. Mukhedkar, and V. Rajagopalan, "A variable frequency soft commutated voltage source inverter delivering sinusoidal waveforms," in *Conference Record of the 1990 IEEE Industry Applications Society Annual Meeting*, IEEE, 1990, pp. 697–702. doi: 10.1109/IAS.1990.152261.

[23] S. Krim, S. Gdaim, A. Mtibaa, and M. F. Mimouni, "Design and implementation of direct torque control based on an intelligent technique of induction motor on FPGA," *Journal of Electrical Engineering and Technology*, vol. 10, no. 4, pp. 1527–1539, Jul. 2015, doi: 10.5370/JEET.2015.10.4.1527.

[24] A. Abbou and H. Mahmoudi, "Real time implementation of a sensorless speed control of induction motor using DTFC strategy," in *2009 International Conference on Multimedia Computing and Systems*, IEEE, Apr. 2009, pp. 327–333. doi: 10.1109/MMCS.2009.5256679.

[25] R. A. El Djallil, H. Kada, G. Yacine, and A. Norediene, "New fuzzy direct torque control optimization for in-wheel motors used in electric vehicle applications," in *2021 12th International Symposium on Advanced Topics in Electrical Engineering (ATEE)*, IEEE, Mar. 2021, pp. 1–8. doi: 10.1109/ATEE52255.2021.9425348.

[26]   A. N. Abdullah and M. H. Ali, "Direct torque control of IM using PID controller," *International Journal of Electrical and Computer Engineering (IJECE)*, vol. 10, no. 1, pp. 617–625, Feb. 2020, doi: 10.11591/ijece.v10i1.pp617-625.

BIOGRAPHIES OF AUTHORS

Moussa Bessike Angon is a Ph.D. student in Energy, Materials, Modelling, and Methods Research Laboratory (LE3M), National Higher Polytechnic School in University of Douala, Cameroon. He was born on February 1980 in Cameroon. In 2018, he graduated with a master 2 research in Telecommunication and Information System in National Higher Polytechnic School in University of Douala, Cameroon. He can be contacted at email: el_moussa_be@yahoo.fr.

Offolé Florence originally from the Eastern region of Cameroon (Africa), Haut-Nyong Department, born March 8, 1982 in Bertoua. She has a course in Mechanical and Production Engineering at ENSAI in Ngaoundéré Cameroon (Africa). In 2017, she obtained the Doctorate/Ph.D. in Mechanics and Production at the University of Douala Cameroon. In her thesis, she develops a method for evaluating the performance of industrial systems based on the use of neuro-fuzzy networks combined with mesh networks. She has been a lecturer since 2022, she focusses her research activities in the field of artificial intelligence, operational safety of systems, prediction, diagnosis, and prognosis of industrial systems. She is also vice-dean of Education and Student Monitoring at the Faculty of Sciences of the University of Bertoua Cameroon and Permanent Teacher at the National Higher Polytechnic School of Douala Cameroon (Africa). She contributes to the development of digital tools and she introduce students from Nationale Supérieure Polytechnique de Douala and the Faculty of Sciences of the University of Bertoua Cameroon. She belongs to the Energy, Modeling, Materials, and Methods Laboratory (E3M) of the University of Douala Cameroon. She can be contacted at email: florenceoffole@yahoo.fr.

Nguiya Severin received his Ph.D. in Physics, which obtained at the National Polytechnic School of the University of Yaoundé I, Cameroun. Geophysical investigation of the Lom volcano-sedimentary basin (East Cameroon): structural and tectonic implications. He is a full professor, of Structural Geophysics, Gravity, Magnetic, and Seismology, in Cameroon. He is a lecturer at the National Polytechnic School of the University of Douala. He published: High-precision structural mapping using Advanced Enhancement Methods of Gravity Anomalies in Southwest Cameroon (Central Africa): Tectonic Implications. He can be contacted at email: nguiyaplus@yahoo.fr.

Mouné Cedric Jordan was born in Douala (Cameroon) in June 1999. In 2021, he graduated with a Master 2 research in Electric Energy and Robotic at the National Advanced School of Engineering of Douala, where he has since pursued a post-graduate study. His field of study is electrical drive systems and power electronics. He can be contacted at email: mouneced157@gmail.com.

Ndoumbé Matéké Max is a lecturer and researcher at the University of Douala, Cameroon. He is the holder of a teacher's diploma of technical high schools' option Electrotechnics obtained in 2012 and a master's degree in Electrotechnics, Electronics, Automation, and Telecommunication at the University of Douala in 2015. In 2022, he obtained a Ph.D. in Engineering Sciences with a specialization in Industrial Electronics and Systems. His research interests are variable frequency electric drives, static converters, and electric vehicles. He can be contacted at email: mdesmax@yahoo.fr.